Published in final edited form as:
J Biol Chem. 2004 March 19; 279(12): 11432–11443.

The SANT2 Domain of the Murine Tumor Cell DnaJ-like Protein 1 Human Homologue Interacts with α_1-Antichymotrypsin and Kinetically Interferes with Its Serpin Inhibitory Activity*

Barbara Kroczynska, **Christina M. Evangelista**, **Shalaka S. Samant**, **Ebrahim C. Elguindi**, and **Sylvie Y. Blond**‡

From the Center for Pharmaceutical Biotechnology, College of Pharmacy, Department of Medicinal Chemistry and Pharmacognosy, University of Illinois, Chicago, Illinois 60607-7173

Abstract

The murine tumor cell DnaJ-like protein 1 or MTJ1/ERdj1 is a membrane J-domain protein enriched in microsomal and nuclear fractions. We previously showed that its lumenal J-domain stimulates the ATPase activity of the molecular chaperone BiP/GRP78 (Chevalier, M., Rhee, H., Elguindi, E. C., and Blond, S. Y. (2000) *J. Biol. Chem*. 275, 19620–19627). MTJ1/ERdj1 also contains a large carboxyl-terminal cytosolic extension composed of two tryptophan-mediated repeats or SANT domains for which the function(s) is unknown. Here we describe the cloning of the human homologue HTJ1 and its interaction with α_1-antichymotrypsin (ACT), a member of the serine proteinase inhibitor (serpin) family. The interaction was initially identified in a two-hybrid screening and further confirmed *in vitro* by dot blots, native electrophoresis, and fluorescence studies. The second SANT domain of HTJ1 (SANT2) was found to be sufficient for binding to ACT, both in yeast and *in vitro*. Single tryptophanalanine substitutions at two strictly conserved residues significantly (Trp-497) or totally (Trp-520) abolished the interaction with ACT. SANT2 binds to human ACT with an intrinsic affinity equal to 0.5 nM. Preincubation of ACT with nearly stoichiometric concentrations of SANT2 wild-type but not SANT2: W520A results in an apparent loss of ACT inhibitory activity toward chymotrypsin. Kinetic analysis indicates that the formation of the covalent inhibitory complex ACT-chymotrypsin is significantly delayed in the presence of SANT2 with no change on the catalytic efficiency of the enzyme. This work demonstrates for the first time that the SANT2 domain of MTJ1/HTJ1/ERdj1 mediates stable and high affinity protein-protein interactions.

The rough endoplasmic reticulum (ER)[1] is the primary site for the synthesis and maturation of secreted and membrane proteins. At this site molecular chaperones and their associated enzymes promote the folding and assembly of newly synthesized polypeptides (1,2). Only native proteins leave the ER to enter the vesicular secretory pathway and reach their appropriate destinations. Misfolded or aberrant proteins are transported back to the cytosol, then transferred to the 26 S proteasome in a process termed ER-associated protein degradation (3–6).

The molecular chaperone immunoglobulin heavy chain-binding protein (BiP)/GRP78, a member of the Hsp70 family resident of the ER, is involved in many cellular processes that

*This work was supported by National Institutes of Health Grant NIHGM 58107 (to S. Y. B.) and the Talaat Basha Family Foundation (to E. C. E.).

‡ To whom correspondence should be addressed: Center for Pharmaceutical Biotechnology (M/C 870), University of Illinois, Molecular Biology Research Bldg., 900 South Ashland Ave., Chicago, IL 60607-7173. Tel.: 312-996-5416; Fax: 312-413-9303; E-mail: blond@uic.edu..

[1]The abbreviations used are: ER, endoplasmic reticulum; ACT, α_1-antichymotrypsin; BiP, immunoglobulin heavy chain-binding protein; HA, hemagglutinin; RSL, reactive site loop; SD, minimal synthetic dropout medium; Succ-AAPF-*p*NA, succinyl-Ala-Ala-Pro-Phe-*p*-nitro-anilide; X-α-gal, 5-bromo-4-chloro-3-indolyl-β-D-galactopyranoside.

include the translocation of newly synthesized polypeptides across the ER membrane, participation in their folding and maturation, assisting in refolding and renaturation, targeting misfolded proteins to the cytosol for proteasomal degradation, maintaining selectivity of the ER membrane by closing the translocon pore, as well as regulating calcium homeostasis (7–10). ATPase activity of BiP is required for most of these processes (11,12). In the ATP-bound form BiP binds to unfolded substrates with low affinity. The hydrolysis of ATP to ADP induces conformational changes that stabilize the BiP-unfolded substrates complexes. The ATPase activity of BiP and other Hsp70 proteins is stimulated by members of the J-domain family (13). In the yeast *Saccharomyces cerevisiae* BiP/Kar2p is assisted by at least three J-domain proteins: Sec63p, Jem1p, and Scj1p (12,14–17). The integral membrane protein Sec63p is an essential component of the ER membrane translocon (18). Jem1p together with BiP/Kar2p are part of a nuclear fusion complex (19,20), and Scj1p is likely to be involved in protein folding and assembly in the ER lumen (17,21). Both Jem1p and Scj1p may also facilitate the retrotranslocation of lumenal ER-associated protein degradation substrates to the cytosol by preventing aggregation of misfolded polypeptides in the ER (12). In mammals, five ER J-domain proteins have been identified so far, all of which stimulate BiP ATPase activity: MTJ1/ERdj1 (22–24), the human Sec63 homologue/ERdj2 (25,26), the Scj1 homologue or HEDJ/ERdj3 (21,27), ERdj4 (28), and ERdj5 (29).

We previously showed that the lumenal J-domain of murine MTJ1 forms a stable complex with BiP and stimulates its ATPase activity at stoichiometric concentrations (23). More recently, Zimmermann and colleagues (24) identified MTJ1 as having higher affinity for BiP than the more abundant Sec63 homologue in dog pancreas. The NH_2-terminal of MTJ1 that carries the J-domain is followed by one transmembrane helix and a cytosolic carboxyl-terminal domain composed of a spacer region that possesses homology with Sec63p flanked by two tryptophan-mediated repeats or SANT domains for which no function has been attributed (23,24). SANT domains are structurally related to the Myb DNA-binding domain (30,31) and are present at one to five copies in a variety of transcription factors or regulators including Swi3, Ada2, N-CoR, TFIIIB (30,32–34) or components involved in chromatin remodeling (35,36). Besides these reports, very little is known about the function of SANT-containing proteins.

In the present study, we have cloned the human homologue of MTJ1, which we call HTJ1, and used its COOH-terminal domain as bait in a two-hybrid screening of a human liver cDNA library. We have identified α_1-antichymotrypsin (ACT), a member of the serpin family, as a potential interacting candidate. Targeted mutagenesis indicates that the second SANT domain of HTJ1 (SANT2) mediates the interaction with ACT and that this interaction can be totally disrupted by a tryptophan to alanine single mutation (W520A). SANT2-ACT interaction was confirmed *in vitro* using purified proteins. ACT once bound to SANT2 was found to have no inhibitory activity toward chymotrypsin. SANT2 significantly slows down the kinetic of formation of the ACT-chymotrypsin acyl complex with no significant effect on the catalytic efficiency of the proteinase. This report documents for the first time that the human homologue of MTJ1/ERdj1 can mediate high affinity protein-protein interactions through its cytosolic domain. In another report, we describe that HTJ1 also interacts with a member of the inter-α-trypsin inhibitor and protects it from being processed by its natural protease.[2] Our data suggests that HTJ1/ERdj1 may play a role in the secretion of protease inhibitors in mammalian cells.

[2]B. Kroczynska, L. Yang, H. Lu, and S. Y. Blond, submitted for publication.

EXPERIMENTAL PROCEDURES

Materials, Antibodies, Proteins, and Strains

All components of the two-hybrid system, including cloning vectors pGBKT7 and pACT2, human liver cDNA library, *S. cerevisiae* strain AH109, anti-c-Myc monoclonal antibody, anti-HA tag polyclonal antibody, X-α-gal, dropout supplements, and cobalt-chelating resin Talon were obtained from Clontech. Bacterial vector pUC19 was from New England BioLabs, Beverly, MA. pET15b plasmid and the BL21(DE3) codon$^+$ strain were from Novagen, Madison, WI. Pfu polymerase was from Stratagene, La Jolla, CA. All restriction enzymes and T4 DNA ligase were from MBI Fermentas, Amherst, NY. The ECL kit was from Amersham Biosciences. Human plasma ACT was from Calbiochem-Novabiochem Corp., San Diego, CA. Bovine pancreas chymotrypsin, and its substrate succinyl-Ala-Ala-Pro-Phe-*p*-nitroanilide (Succ-AAPF-*p*NA) were from Sigma. Monoclonal anti-α_1-antichymotrypsin antibody was obtained from Fitzgerald Industries International, Inc. Concord, MA.

Cloning of HTJ1 cDNA

A nucleotidic sequence from a 10-week-old human embryo (AK027263, GI: 14041830) coding for a putative MTJ1 homologue was used as a template to design the set of primers for the amplification of a human liver cDNA library. The forward primer (5′-ATGACGGCTCCTTGCTCCCAG-3′) and reverse primer (5′-TCAGCTTTTAGCTTGTTTTTTCTTTTGGACC-3′) were used in PCR with Pfu polymerase. The PCR product (1700 bp) was then subcloned into the SmaI site of pUC19. The construct (pUCHTJ1) was sequenced on both strands and sequence analysis was carried out using BLAST sequence analysis software.

Yeast and Bacterial Plasmids

cDNA coding for HTJ1, full-length ACT, and fragments were amplified by PCR using the forward and reverse primers listed in Table I. PCR products were subcloned in the yeast pGBKT7 plasmid, in-frame with the NH_2-terminal GAL4 DNA-binding domain and the c-Myc epitope tag (pGBKT7 constructs, Table I). A number of PCR products containing varying lengths of HTJ1 and full-length ACT cDNA were cloned in pET15b *Escherichia coli* expression vector in-frame with a NH_2-terminal hexahistidine tag (p$(His)_6$ constructs, Table I). Finally two PCR products of ACT coding the $ACT_{344–400}$ and $ACT_{35–343}$ fragments were fused to the NH_2-terminal GAL4 activation domain and the HA epitope tag of the yeast pACT2 plasmid (pACT2 constructs, Table I). The clone pGBKT7/$HTJ1_{242–493}$ was generated by digestion of pGBKT7/$HTJ1_{242–554}$ with PstI and religation. The $HTJ1_{493–554}$:W497A mutant was engineered using PCR and a forward mutagenic primer (Table I). The $HTJ1_{493–554}$:W520A mutant was created using the QuikChange site-directed mutagenesis kit (Stratagene) and two overlapping mutagenic primers (Table I). The construct pGBKT7/$HTJ1_{493–554}$:W497A was used as a template to generate the double mutant pGBKT7/$HTJ1_{493–554}$:W497A,W520A. The constructs pGBKT7/pGBKT7/$HTJ1_{493–554}$, pGBKT7/$HTJ1_{493–554}$:W497A, $HTJ1_{493–554}$:W520A, and pGBKT7/$HTJ1_{493–554}$:W497A,W520A were digested with NdeI and XhoI and the inserts were ligated into pET15b to generate p$(His)_6HTJ1_{493–554}$, p$(His)_6HTJ1_{493–554}$:W497A, p$(His)_6$-$HTJ1_{493–554}$:W520A, and p$(His)_6HTJ1_{493–554}$:W497A,W520A, respectively. All constructs were sequenced.

Yeast Two-hybrid Library Screening

The construct pGBKT7/$HTJ1_{242–554}$ (*TRP1*) was used as bait to screen a human liver cDNA library fused to the pACT2 (*LEU2*) GAL4-activation domain and the HA epitope tag. The bait pGBKT7/$HTJ1_{242–554}$ and the library-containing target pACT2 vector were sequentially transformed into the two-hybrid yeast strain AH109 as described (38). As strain AH109

possesses three reporter genes (*ADE2*, *HIS3*, and *MEL1*) that are under the control of the Gal4 upstream activating sequences and TATA boxes, transformants were grown on minimal synthetic dropout four medium lacking tryptophan (Trp), leucine (Leu), histidine (His), and adenine (Ade) (SD/−Trp/−Leu/−His/−Ade) to select for potential interactors. Approximately 2×10^6 clones, representing 1/3 library equivalents, were screened against the pGBKT7/$HTJ1_{242–554}$ bait. Transformants with the ability to grow on SD/−Trp/−Leu/−His/−Ade that turned blue in the presence of X-α-gal were analyzed further as described under "Results."

Western Blot Analysis of Protein Expression in Yeast Protein Extracts

The yeast strain AH109 was transformed separately with pGBKT7 or pACT2-derived constructs (Table I) and grown overnight on selective SD medium at 30 °C. The yeast protein extracts were prepared according to the manufacturer's procedure (Clontech, protocol number PT3024-1, version PR91200). Following electrophoresis on a 10% SDS-PAGE gel, proteins were transferred onto nitrocellulose membrane in 50 mM Tris (pH 8.0), 380 mM glycine, 0.1% SDS, and 20% methanol (transfer buffer). The recombinant proteins expressed from pGBKT7-derived constructs were detected using an anti-c-Myc monoclonal primary antibody and an anti-mouse conjugated to horseradish peroxidase secondary antibody. The expression of the pACT2-derived fusion proteins was detected by using a rabbit polyclonal antibody to HA. Immunoreactivity was visualized by enhanced chemiluminescence using the ECL kit.

Expression and Purification of Recombinant Proteins

The recombinant histidine-tagged proteins were expressed from pET15-derived constructs (Table I). The *E. coli* BL21(DE3) $codon^+$ cells were grown at 37 °C in Luria broth (LB) supplemented with carbenicillin at 100 μg/ml final concentration. Synthesis of recombinant proteins was induced by addition of isopropyl-1-thio-β-D-galactopyranoside at 0.4 mM final concentration at mig-log exponential phase (A_{600} ~ 0.5–0.6). Cells were harvested after a 16-h induction, lysed using a French press at 10,000 p.s.i., and the histidine-tagged protein was purified on cobalt-chelating resin as described by the manufacturer (Talon resin, Clontech). All recombinant proteins were expressed in the soluble fraction except for His_6-$ACT_{1–400}$, which accumulates in inclusion bodies and was purified from lysate pellets resolubilized in 20 mM Tris (pH 8.0), 8M urea, 100 mM NaCl and purified in denaturing conditions. Fractions eluted from the resin were dialyzed overnight at 4 °C in 20 mM Tris (pH 8.0), 100 mM NaCl to promote renaturation. The renatured soluble recombinant ACT was further purified by fast pressure liquid chromatography using gel filtration on Superdex 75 (Amersham Biosciences) equilibrated in the same buffer. Protein concentrations were estimated by the method of Bradford (39). Protein purity and homogeneity were analyzed by PAGE performed in both denaturing and native conditions (40).

Dot Blot Protein Analysis

Dot blots were performed as described (41) with the following modifications. Various amounts of recombinant His_6-HTJ1 proteins were applied onto a nitrocellulose membrane, dried, then incubated overnight with a solution of soluble renatured His_6-$ACT_{1–400}$ (5 μg/ml) in 20 mM Tris-Cl (pH 8.0), 150 mM NaCl. After washing in phosphate-buffered saline, bound ACT was detected with an anti-human ACT monoclonal antibody (1:20,000). In control experiments, purified His_6-J-MTJ1 and His_6-J-MTJ1:H89Q prepared as described (23) were applied to the nitrocellulose membrane, and incubated with a solution of recombinant His_6-BiP (5 μg/ml) in Tris-Cl (pH 8.0), 150 mM NaCl. Bound BiP was detected by chemiluminescence using a commercially available anti-BiP antibody (PAI-014, Affinity Bioreagents Inc., Golden, CO). In all experiments, immunoreactivity was visualized by ECL.

Native PAGE and Immunodetection of ACT-HTJ1 Interaction

Human plasma ACT (0.64 μM) was incubated at 25 °C with increasing concentrations of purified His_6-$HTJ1_{493–554}$ wild-type or mutant (His_6-Tris (pH 8.0), 100 mM NaCl prior to $HTJ1_{493–554}$:W497A) in 20 mM electrophoresis in non-denaturing conditions (40). ACT was detected by Western blotting using a commercially available monoclonal antibody.

Tryptophan Fluorescence Quenching Measurements

All measurements were carried out on a Cary Eclipse fluorescence spectrophotometer at a temperature of 25 °C regulated by a thermostatted cell holder and a Cary PCB15 Water peltier system (Varian Instruments, Walnut Creek, CA). All data were analyzed using the Cary Eclipse software (Varian Instruments). The emission spectra were recorded between 300 and 450 nm at an excitation wavelength of 280 nm. The excitation and emission slits were set to 10 nm. The emission wavelength increment was 4 nm and the acquisition time 3 s. Tryptophan fluorescence intensities were corrected for the contribution of ACT alone analyzed in the same conditions of temperature, buffer (20 mM Tris (pH 8.0), 100 mM NaCl), and concentrations. In titration experiments, the fraction of ACT bound to SANT2 (4 nM) at every serpin concentration (0–16 nM) was calculated relative to the fluorescence intensity (excitation wavelength = 280 nm; emission wavelength = 350 nM) at saturating concentrations of ACT (100% bound) minus the intensity of SANT2 alone (0% bound). The intrinsic dissociation equilibrium constant, K_{diss}, was determined using the Scatchard representation corresponding to the equation,

$$[\mathrm{ACT}]b/[\mathrm{ACT}]f = -1/K_{diss} + [\mathrm{ACT}]b + n[\mathrm{SANT2}]_{Tot}/K_{diss} \quad \text{(Eq. 1)}$$

where [ACT]*b* represents the concentration of bound ACT; [ACT]*f* is the concentration of free ACT; *n* is the number of SANT2 binding site(s) per ACT molecule. Plot of [ACT]*b*/[ACT]*f* = *f*([ACT]*b*) gives a straight line with a negative slope that equals $-1/K_{diss}$ and extrapolation on the *x* axis gives the maximum concentration of bound ACT and is used to deduce the stoichiometry of the complex. As SANT2 and ACT contain two and three tryptophans, respectively, we used Lehrer representation to determine the fraction of tryptophan residues quenched upon SANT2-ACT interactions as described (42), using the equation,

$$F_0/F_0 - F = 1/f_a K[\mathrm{ACT}] + 1/f_a \quad \text{(Eq. 2)}$$

where F_0 is the tryptophan fluorescence of SANT2 alone; *F* is the tryptophan fluorescence of the SANT2-ACT complex at a given ACT concentration [ACT]; f_a is the maximum fraction of accessible fluorophore; *K* is the Lehrer quenching constant of an individual tryptophan. The Lehrer representation $F_0/F_0 - F = f(1/[\mathrm{ACT}])$ gives a straight line whose extrapolation on the *y* axis ([ACT] = 0) corresponds to the value of $1/f_a$ (42).

Chymotrypsin Activity

All steady state experiments were carried out at 25 °C in 20 mM Tris (pH 8.0), 100 mM NaCl with the chromogenic substrate Succ-AAPF-*p*NA. Absorbance was recorded spectrophotometrically at 405 nm. K_m and V_{max} were determined using the Lineweaver-Burk representation and the Michaelis-Menten equation at 4 nM chymotrypsin, substrate ranged from 0 to 0.1 mM, in the absence or presence of 4 nM SANT2. The catalytic constant, k_{cat}, was determined for 0.2–5.0 nM chymotrypsin in the presence of 0.1 mM Succ-AAPF-*p*NA. To determine the residual activity of chymotrypsin in the presence of the preformed ACT-SANT2 complex, human plasma ACT (4.0 nM) was preincubated for 20 min at 25 °C in the presence of 0–640 nM His_6-$HTJ1_{493–554}$, His_6-$HTJ1_{493–554}$:W497A, or His_6-$HTJ1_{493–554}$:W497A, W520A and 0.1 mM Succ-AAPF-*p*NA prior to the addition of chymotrypsin (4.0 nM final

concentration). The residual chymotrypsin activity was measured for 5–10 min at 15-s intervals. The percentage of inhibition was normalized to the activity of chymotrypsin alone (100%). Kinetic analysis of ACT inhibition of chymotrypsin in the presence or absence of SANT2 was performed as described (43) with the following modifications. Equimolar concentrations of chymotrypsin and ACT (4 nM) were incubated 0–10 min and the residual chymotrypsin activity was measured at timed intervals after addition of 0.1 mM Succ-AAPF-*p*NA. The concentration of free chymotrypsin [E_f] was estimated using a standard curve of chymotrypsin activity. Using the equation,

$$1/[E_f] - k_{ass}(t) + 1/[E_0] \quad \text{(Eq. 3)}$$

a plot of 1/[E_f] *versus* time yields a straight line with a slope equal to the association rate constant, k_{ass}, and an *x* intercept corresponding to 1/[E_o] or the total concentration of the enzyme. The same experiments were repeated with a 20-min preincubation period in the presence of equimolar concentrations of SANT2 (4 nM) prior to the addition of chymotrypsin.

RESULTS

Isolation, Sequence Analysis of cDNA Encoding the HTJ1, and Amino Acid Sequence Similarities of HTJ1 and MTJ1

The human homologue of MTJ1/ERdj1 was cloned from a human liver cDNA library (see "Experimental Procedures") (AY225122) and found to be 84% identical to the murine protein (Fig. 1). An NH_2-terminal signal sequence containing a putative cleavage site between amino acids 47 and 48 could target the signature J-domain (residues 63–138) to the lumen of the endoplasmic reticulum where it can interact with BiP (22–24). The J-domain is followed by a membrane anchor, a cytosolic NH_2-terminal region that may interact with ribosomes (residues 173–239) as observed in the murine homologue MTJ1 (24), and a large cytosolic domain consisting of three additional subdomains or regions, namely two SANT domains (SANT1 residues 325–377 and SANT2 residues 493–545), also called tryptophan-mediated repeats, separated by a 116-residue long spacer that includes a region (residues 409–465) that exhibits 28% identity with Sec63p. A KK*XX*-like tail motif would account for HTJ1 retrieval from the Golgi to the ER and its retention, as observed for other type 1 membrane proteins (44–46).

Interaction of HTJ1 with ACT Detected by the Two-hybrid System in Yeast

The liver is an organ important in the secretion of many plasma proteins and molecular chaperones involved in these processes, such as BiP and possibly HTJ1, are particularly abundant in liver microsomes. To elucidate the function of HTJ1 in secreting cells, we used a yeast two-hybrid system and screened a human liver cDNA library for proteins that interact with the carboxyl-terminal $HTJ1_{242–554}$ fragment (Fig. 2*A*). Prior to screening, the yeast strain AH109 transformed with the vector pGBKT7/$HTJ1_{242–554}$ (Table I) and the empty pACT2 vector was shown to be transcriptionally inert by nutrition selection (data not shown). The $HTJ1_{242–554}$ fragment was efficiently expressed in-frame with the *Gal4* DNA-binding domain and the c-Myc epitope, as indicated by the size of the fusion protein and its immunoreactivity toward an anti-c-Myc antibody (Fig. 2B). Next, the pGBKT7/$HTJ1_{242–554}$ was used as bait for the screening of a human liver cDNA library cloned in the pACT2 plasmid. Initially, 23 yeast clones induced the expression of the three reporter genes (*HIS3*, *ADE2*, and *MEL1*), indicated by growth on SD dropout four medium and blue staining in the presence of X-α-gal. Of these, 15 were eliminated from further studies because the isolated plasmids re-transformed in the AH109 strain activated the reporter genes in the absence of the bait. Putative interacting targets were identified by DNA sequencing. Four clones corresponded to metallothionein (BC008408), a protein that has been isolated in numerous screens and is thus involved in multiple, non-specific interactions (41).[3] One clone designated pACT2/$ACT_{140–400}$ (Fig. 3*A*)

contained a large insert coding for residues 140–400 of the ACT (AF089747) (47) in the same reading frame as the NH_2-terminal *Gal4* activation domain and the HA epitope tag of the pACT2 vector (Fig. 3*B*). The yeast strain AH109 co-transformed with pACT2/$ACT_{140–400}$ and the vector pGBKT7/53 did not grow on the selective medium, SD/−Trp/−Leu/−His/−Ade/X-α-gal (Fig. 4, *last lane*), indicating that clone pACT2/$ACT_{140–400}$ could not activate the reporter gene system on its own and that ACT may represent a true HTJ1-interacting protein.

ACT Interacts with the SANT2 Domain of HTJ1

The region of HTJ1 responsible for interaction with ACT was further characterized *in vivo* and a number of HTJ1 variants were engineered including a SANT2-less (pGBKT7/$HTJ1_{242–493}$), a SANT2-only (pGBKT7/$HTJ1_{493–554}$), and SANT1-only fusion proteins (pGBKT7/$HTJ1_{242–411}$)(Fig. 2*A* and Table I). Efficient expression of each fusion protein in yeast extracts was detected by immunoblot using the c-Myc antibody (Fig. 2*B*). Yeast strain AH109 co-transformed with pACT2$_{140–400}$ and all pGBKT7-derived constructs grows on medium lacking leucine and tryptophan (Fig. 4), indicating that the two plasmids are efficiently propagated in those conditions. However, the strain can only grow on SD/−Trp/−Leu/−His/−Ade medium and form blue colonies in the presence of X-α-gal with constructs that express the SANT2 domain (residues 493–554) (Fig. 4). Control plasmids expressing the lumenal J-domain of HTJ1 (pGBKT7/$JHTJ1_{45–148}$) or the p53 antigen (pGBKT7/53) do not sustain growth on selective medium when co-expressed with the $ACT_{140–400}$ fragment (Fig. 4). Additionally, the single substitution of the highly conserved tryptophan residue at position 520 by alanine within the SANT2 domain totally abolished the transcription of the reporter genes (pGBKT7/$HTJ1_{493–554}$: W520A, Fig. 4), and the same substitution at position 497 greatly destabilizes the complex because only marginal growth was observed (pGBKT7/$HTJ1_{493–554}$:W497A, Fig. 4). As expected, the double mutant is transcriptionally inactive (pGBKT7/$HTJ1_{493–554}$:W497A,W510A, Fig. 4). Expression of the reactive site loop (RSL) (pACT2/$ACT_{344–400}$) is not sufficient for growth on selective medium and its deletion (pACT2/$ACT_{35–343}$, Fig. 4) does not abolish interaction with SANT2. These results indicate that the SANT2 domain of HTJ1 interacts with a region in ACT comprised between residues 140 and 343 that does not overlap with the RSL and does not require structural integrity of the serpin.

HTJ1-ACT Interaction in Vitro

Next, we tested whether SANT2 could also interact with full-length ACT *in vitro*. Recombinant His_6-$HTJ1_{242–554}$, His_6-$HTJ1_{242–377}$, His_6-$HTJ1_{378–492}$, His_6-$HTJ1_{493–554}$, His_6-$HTJ1_{493–554}$:W497A, His_6-$HTJ1_{493–554}$:W520A, His_6-$HTJ1_{493–554}$:W497A,W520A, and $His_6ACT_{1–400}$ (Table I) were produced in *E. coli* and purified by affinity chromatography on cobalt chelating resin (Fig. 5). Decreasing amounts of purified HTJ1 substrate proteins were immobilized onto nitrocellulose and bound recombinant uncleaved ACT was detected using a highly specific anti-human ACT antibody (Fig. 6). The results indicate that among all the substrates tested, only His_6-$HTJ1_{242–554}$ and His_6-$HTJ1_{493–554}$ strongly bind to ACT (Fig. 6*A*, *lanes 1* and *4*, respectively). As observed *in vivo*, the $HTJ1_{493–554}$:W497A mutant interacts weakly with ACT (Fig. 6*A*, *lane 5*), and the $HTJ1_{493–554}$:W520A mutant does not (Fig. 6, *lane 6*). In our conditions, the dot blot test appears to be highly specific as BiP binding was detected with J-MTJ1 (Fig. 6*B*, *lane 1*), but not with the mutant J-MTJ1:H89Q (Fig. 6*B*, *lane 2*), as observed in our earlier studies (23).

We then analyzed the interaction of SANT2 with human plasma-glycosylated ACT, using native electrophoresis and Western blot (Fig. 7). A SANT2-ACT complex is readily detectable as a low migrating species on native polyacrylamide gels (Fig. 7*A*, *lane 2*), and all ACT is

[3]B. Kroczynska, L. King, E. C. Elguindi, and S. Y. Blond, unpublished observations.

bound in the presence of five molar excess or more of SANT2 (Fig. 7*A*, *lanes 4–8*). A complex also forms in the presence of SANT2:W497A (Fig. 7*B*), but less efficiently as not all ACT was trapped in the presence of 80 molar excess of SANT2 mutant (Fig. 7*B*, *lane 8*). In these conditions, no complex was observed for the double mutant His_6-$HTJ1_{493–554}$:W497A,W520A. Complexes cannot be detected by SDS-PAGE, indicating that the interaction is not SDS-resistant (data not shown).

Interaction of SANT2 with ACT is accompanied by a decrease in SANT2 tryptophan fluorescence (Fig. 8*A*). The fluorescence signal declines with increasing concentrations of ACT until a plateau is reached at saturating concentrations of serpin (Fig. 8*B*). Using Scatchard representation and equations (see "Experimental Procedures"), we determined that the SANT2-ACT complex forms with an intrinsic affinity equal to 0.5 n_M and a serpin-SANT2 stoichiometry of 1:1 (Fig. 8*C*). SANT2 and ACT contain two and three tryptophan residues, respectively. Using the Lehrer representation (Fig. 8*D*) and the equations described under "Experimental Procedures," we calculated that the fraction of accessible tryptophan f_a equals 0.2, indicating that only one tryptophan residue of the five present contributes to the change in fluorescence observed upon ACT-SANT2 interaction. Similar experiments repeated with the SANT2:W520A mutant did not give any fluctuation in signal upon ACT addition. Taken together these data indicate that SANT2 binds to ACT at one site, with an affinity in the sub-nanomolar range and that Trp-520 is crucial to mediate this interaction and contribute to most of the fluorescence quenching signal.

SANT2 Alters ACT Inhibitory Activity

We next investigated whether the $HTJ1_{493–554}$ fragment interferes with the ACT inhibitory activity toward chymotrypsin. Indeed, equimolar concentrations of ACT totally inhibits chymotrypsin protease activity (Fig. 9*A*), whereas 160 molar excess of His_6-$HTJ1_{493–554}$ (SANT2) wild-type or mutant had no effect on the serine protease activity (data not shown). Preincubation of ACT with increasing concentrations of the SANT2 fragment prevents ACT from exerting its inhibitory activity toward chymotrypsin (Fig. 9). Half-maximal chymotrypsin activity was restored at an ACT:SANT2 molar ratio equal to about 1:10. In similar conditions, the mutant His_6-$HTJ1_{493–554}$:W497A restores about 50% of the activity, whereas the double mutant His_6-HTJ1493_554:W497A,W520A has no effect, even when present in a very large molar excess over ACT (Fig. 9*B*). SANT2 does not alter the catalytic properties of chymotrypsin and both K_m and k_{cat} remained unchanged (Table II).

SANT2 Delays the Formation of the ACT-Chymotrypsin Complex

Inhibition of the serine proteinase activity by serpin occurs with formation of an irreversible proteinase-serpin complex. This structure is stabilized by insertion of the cleaved NH_2-terminal of the reactive site loop into β-sheet A (48). We examined the kinetics of formation of the ACT-chymotrypsin complex in the presence of millimolar concentrations of the chromogenic substrate. Incubation of equimolar concentrations of ACT and chymotrypsin (0.7 μ_M) leads to a SDS-resistant complex that quickly accumulates within the 5-s to 1-min time range (Fig. 10*A*). A band slightly faster than free ACT is also noticeable after 1 min and most likely corresponds to cleaved ACT. When ACT was preincubated with 20 molar excess SANT2, the formation of the ACT-chymotrypsin complex is considerably delayed, accumulating only after 1 min and remaining incomplete after 10 min of incubation (Fig. 10*B*). Higher concentrations of SANT2 lead to more pronounced delays and barely any ACT-chymotrypsin complex could be detected in the presence of 80 molar excess of SANT2 over ACT (data not shown). The same experiments performed with the SANT2:W497A variant indicate that the mutant also delays the formation of the inhibitory ACT-chymotrypsin complex, although less efficiently than the wild-type SANT2 domain as some ACT-chymotrypsin complex appears after 20 s of incubation (Fig. 10*C*). In all experiments the amount of SANT2 remains unchanged, indicating

that wild-type and mutant SANT2 are not substrates for chymotrypsin in these conditions and do not compete with ACT or the chromogenic substrates for binding to the proteinase. Finally, the rate constant of association between ACT and chymotrypsin is about two times slower in the presence of SANT2 (Fig. 11, Table II). These results are consistent with our observations that incubation of human plasma ACT with SANT2 results in an apparent loss of ACT inhibitory activity because of a delay in the formation of the ACT-chymotrypsin suicide inhibitory complex. The mutant SANT2:W497A has reduced affinity for ACT, allowing more rapid release of the free serpin that can readily inactivate the proteinase in our assay conditions.

DISCUSSION

In mammals, BiP is a molecular chaperone resident of the ER that can potentially interact with at least five J-domain accessory proteins recently renamed ERdj1–5 (21–29). MTJ1/ERdj1 is a class III membrane co-chaperone that interacts with BiP in dog microsomes (24) and stimulates its ATPase activity *in vitro* (23). Apart from the lumenal J-domain that mediates the interaction with BiP (23), MTJ1/ERdj1 contains a highly charged region adjacent to the transmembrane helix that binds to ribosomes and modulates the rate of translation of newly synthesized polypeptides (24). In addition, MTJ1/ERdj1 possesses a large carboxyl-terminal extension composed of two SANT domains and a spacer region for which the function was completely unknown. In the present study, we report the cloning of the human homologue HTJ1 (Fig. 1) and the critical role of its distal SANT domain (SANT2) in the formation of a stable complex with the serpin ACT. In another report,[2] we show that the HTJ1 SANT2 domain also interacts with ITIH4, a member of the inter-α-trypsin inhibitor, reinforcing the concept that HTJ1 may be involved in multiple protein-protein interactions on both sides of the endoplasmic reticulum membrane. Its lumenal J-domain interacts with the molecular chaperone BiP (23), whereas its cytosolic domain may interact with ribosomes (24) and newly translated polypeptides.

The biochemical and kinetic studies presented in this article show that SANT2 delays the formation of the ACT-chymotrypsin acyl complex (Fig. 9) and slows down the kinetics of association between ACT and chymotrypsin without affecting the catalytic properties of the enzyme (Fig. 10, Table II). A general model for the function of serpins based on their physical properties, mechanism, and structure has been established and recently described in fine detail (48,49). In addition to chymotrypsin, ACT inhibits the serine proteases cathepsin G, mast cell chymase, and proenkephalin processing enzymes (50–53). ACT, like other serpins, is characterized by a mobile RSL that is a substrate for the protease, and a dominant β-sheet A that can open to insert the cleaved active site loop or bind exogenous free peptides of the same or similar sequence (50,54–56). Herein we present evidence that SANT2 binds to ACT within a region (residues 140–343) that does not overlap with the RSL itself (Fig. 4) and that the resulting SANT2-ACT complex no longer exhibits inhibitory activity toward chymotrypsin (Figs. 8 and 9). The SANT2-ACT complex is very stable and forms with a dissociation constant equal to K_{app} = 0.5 nM for 4 nM ACT, a value that is about 4 order of magnitude smaller than the average serpin plasma concentration (around 45 mg/100 ml or 7 mM) in healthy individuals (57).

ACT is an abundant serum glycoprotein that is produced by liver cells through the secretory pathway. The ACT precursor contains a signal peptide (Fig. 3*A*) that is cleaved upon translocation across the ER membrane. Glycosylation occurs in the ER prior to transport to the Golgi apparatus and fusion of secretory vesicles with the plasma membrane. Interestingly, HTJ1 can rescue the thermosensitive phenotype of a Sec63 translocation-deficient mutant,[4] suggesting that HTJ1 functions in protein translocation across the endoplasmic reticulum

[4]B. Kroczynska, J. Brodsky, and S. Y. Blond, unpublished data.

membrane. Because a small positively charged region distal of the COOH-terminal of MTJ1 is associated with ribosomes (24), newly translated ACT may associate with HTJ1 through the SANT2 domain prior to its translocation across the ER. We attempt to detect ACT-HTJ1 complexes in membrane fractions prepared from non-transfected hepatocarcinoma HepG2 cells, or transfected with a vector that overexpresses MTJ1 (58). Unfortunately, ACT has a size similar to the heavy chain of immunoglobulins used in the immunoprecipitation experiments and could not be detected under these conditions.[5] It is thus unclear whether or not MTJ1/ERdj1 can stably interact with ACT *in vivo*. In mammalian cells, translocation is a co-translational process and the complex between ERdj1 and ACT may be too short-lived to be detected.

A carboxyl-terminal fragment of MTJ1 was originally found in nuclear extracts (22), and localizes to the nucleus when expressed on its own in COS-7-transfected cells (58). The molecular mechanisms that generate the MTJ1 truncated nuclear form are unclear and remain under investigation in our laboratory. The Sec63-like region that separates the two SANT domains contains a putative nuclear localization signal (R_{439}PRRRK, Fig. 1) that could target the soluble fragment to the nucleus. Interestingly, ACT also localizes in cell nuclei (59,60) but does not possess any putative nuclear localization signal. ACT also has the unique property to bind DNA through exposed lysine residues with no effect on its protease inhibitory activity (61). ACT-DNA interaction is believed to play a role in tumor cell protection and in modulating the activity of chymotrypsin-like enzymes in chromatin (62). However, very little has been done in this area and the role of ACT DNA binding activity in the nucleus remains unknown. Interestingly, two recent reports (63,64) describe that a developmentally regulated serpin, the myeloid and erythroid nuclear termination stage-specific protein or MENT, also localizes to the nucleus and exerts a role in chromatin remodeling. It is very tempting to propose that the interaction of MTJ1 with ACT could mediate membrane release and nuclear localization of the complex and regulation of gene transcription through the DNA binding activity of ACT itself or through protein-protein interactions mediated by the HTJ1 SANT domain(s). Studies are underway to further characterize the role of HTJ1 in ACT secretion, function, and organelle targeting.

SANT domains are reminiscent of tryptophan-mediated DNA binding repeats and are found in many proteins, only few of which have been studied such as MIDA-1, a murine J-domain protein involved in cell growth (65–67), the Zuotin-related factors (68–70), the proto-oncogene c-*myb* (71), the M-phase phosphoprotein 11 (72), Ada2 (33), and the histone-associated CoREST and Mta-L1 (34). The arrangement of the two SANT domains in MTJ1, separated by a 116-residue spacer, is similar to that in CoREST (32,34), N-CoR, and SMRT (37). In the case of N-CoR and SMRT, the SANT domains not only interact with HDAC3 (histone deacetylase 3) but also activate its deacetylase activity (36,37). The yeast and human Ada2p are found in histone acetyltransferase complexes and their SANT domains are important for acetylation of histone NH_2-terminal tails (33,35). Although highly homologous, SANT1 and SANT2 are not interchangeable and ACT has no affinity for SANT1. Although our screen was performed with the complete cytosolic region of HTJ1, no SANT1-interacting protein has been identified so far. Protein modeling of HTJ1 SANT1 and SANT2 domains indicate that although the overall folds are very similar, surface residues are much more polar in SANT1 than they are in SANT2.[2] These differences may be sufficient to control the specificity and thus the function of HTJ1 SANT domains. This hypothesis is currently being tested in our laboratory.

Aromatic residues are highly conserved in all SANT-containing proteins (30) and are important for their function. For example, substitution of tryptophans to alanine in Ada2 leads to a SAGA complex partially defective for nucleosome acetylation (33) and greatly reduces the sequence-

[5]S. Y. Blond, unpublished data.

specific DNA binding activity of c-*myb* (71). We clearly show here that tryptophan 520 is critical for the formation of the SANT2-ACT complex, whereas the other tryptophan residue (Trp-497) appears to be more closely engaged in the interactions with ITIH4.[2] In both cases, however, substitution of the other tryptophan by an alanine greatly decreases the affinity for the substrate. These observations indicate that the HTJ1 SANT2 domain can interact with several target proteins through overlapping but somehow distinct surface areas.

Acknowledgements

We are very grateful to Dr. Peter Gettins, University of Illinois, for critical reading of the manuscript and Dr. Andrew Mesecar, University of Illinois, for helpful discussions. We thank Dr. Joel Zupicich for the kind gift of MTJ1 expressing mammalian vectors.

References

1. Lamande SR, Bateman JF. Semin Cell Dev Biol 1999;10:455–464. [PubMed: 10597628]
2. Fewell SW, Travers KJ, Weissman JS, Brodsky JL. Annu Rev Genet 2001;35:149–191. [PubMed: 11700281]
3. Zhang Y, Nijbroek G, Sullivan ML, McCracken AA, Watkins SC, Michaelis S, Brodsky JL. Mol Biol Cell 2001;12:1303–1314. [PubMed: 11359923]
4. Werner ED, Brodsky JL, McCracken AA. Proc Natl Acad Sci U S A 1996;93:13797–13801. [PubMed: 8943015]
5. McCracken AA, Brodsky JL. J Cell Biol 1996;132:291–298. [PubMed: 8636208]
6. Brodsky JL, Werner ED, Dubas ME, Goeckeler JL, Kruse KB, McCracken AA. J Biol Chem 1999;274:3453–3460. [PubMed: 9920890]
7. Lievremont JP, Rizzuto R, Hendershot L, Meldolesi J. J Biol Chem 1997;272:30873–30879. [PubMed: 9388233]
8. Gething MJ. Semin Cell Dev Biol 1999;10:465–472. [PubMed: 10597629]
9. Stronge VS, Saito Y, Ihara Y, Williams DB. J Biol Chem 2001;276:39779–39787. [PubMed: 11514579]
10. Haigh NG, Johnson AE. J Cell Biol 2002;156:261–270. [PubMed: 11807091]
11. Corsi AK, Schekman R. J Biol Chem 1996;271:30299–30302. [PubMed: 8939984]
12. Nishikawa SI, Fewell SW, Kato Y, Brodsky JL, Endo T. J Cell Biol 2001;153:1061–1070. [PubMed: 11381090]
13. Kelley WL. Curr Biol 1999;9:305–308.
14. Scidmore MA, Okamura HH, Rose MD. Mol Biol Cell 1993;4:1145–1159. [PubMed: 8305736]
15. Corsi AK, Schekman R. J Cell Biol 1997;137:1483–1493. [PubMed: 9199165]
16. Nishikawa S, Endo T. J Biol Chem 1997;272:12889–12892. [PubMed: 9148890]
17. Silberstein S, Schlenstedt G, Silver PA, Gilmore R. J Cell Biol 1998;143:921–933. [PubMed: 9817751]
18. Johnson AE, van Waes MA. Annu Rev Cell Dev Biol 1999;15:799–842. [PubMed: 10611978]
19. Nishikawa S, Endo T. Biochem Biophys Res Commun 1998;244:785–789. [PubMed: 9535743]
20. Brizzio V, Khalfan W, Huddler D, Beh CT, Andersen SS, Latterich M, Rose MD. Mol Biol Cell 1999;10:609–626. [PubMed: 10069807]
21. Bies C, Guth S, Janoschek K, Nastainczyk W, Volkmer J, Zimmermann R. Biol Chem 1999;380:1175–1182. [PubMed: 10595580]
22. Brightman SE, Blatch GL, Zetter BR. Gene (Amst) 1995;153:249–254. [PubMed: 7875597]
23. Chevalier M, Rhee H, Elguindi EC, Blond SY. J Biol Chem 2000;275:19620–19627. [PubMed: 10777498]
24. Dudek J, Volkmer J, Bies C, Guth S, Muller A, Lerner M, Feick P, Schafer KH, Morgenstern E, Hennessy F, Blatch GL, Janoscheck K, Heim N, Scholtes P, Frien M, Nastainczyk W, Zimmermann R. EMBO J 2002;21:2958–2967. [PubMed: 12065409]
25. Skowronek MH, Rotter M, Haas IG. Biol Chem 1999;380:1133–1138. [PubMed: 10543453]

26. Tyedmers J, Lerner M, Bies C, Dudek J, Skowronek MH, Haas IG, Heim N, Nastainczyk W, Volkmer J, Zimmerman R. Proc Natl Acad Sci U S A 2000;97:7214–7219. [PubMed: 10860986]
27. Yu M, Haslam RH, Haslam DB. J Biol Chem 2000;275:24984–24992. [PubMed: 10827079]
28. Shen Y, Meunier L, Hendershot LM. J Biol Chem 2002;277:15947–15956. [PubMed: 11836248]
29. Cunnea PM, Miranda-Vizuete A, Bertoli G, Simmen T, Damdimopoulos AE, Herman S, Leinonen S, Pelto Huikko M, Gustafsson JA, Sitia R, Spyrou G. J Biol Chem 2003;278:1059–1066. [PubMed: 12411443]
30. Aasland R, Stewart AF, Gibson T. Trends Biochem Sci 1996;21:87–88. [PubMed: 8882580]
31. Hanaoka S, Nagadoi A, Yoshimura S, Aimoto S, Li B, de Lange T, Nishimura Y. J Mol Biol 2001;312:167–175. [PubMed: 11545594]
32. Andres ME, Burger C, Peral-Rubio MJ, Battaglioli E, Anderson ME, Grimes J, Dallman J, Ballas N, Mandel G. Proc Natl Acad Sci U S A 1999;96:9873–9878. [PubMed: 10449787]
33. Sterner DE, Wang X, Bloom MH, Simon GM, Berger SL. J Biol Chem 2002;277:8178–8186. [PubMed: 11777910]
34. Humphrey GW, Wang Y, Russanova VR, Hirai T, Qin J, Nakatani Y, Howard BH. J Biol Chem 2001;276:6817–6824. [PubMed: 11102443]
35. Boyer LA, Langer MR, Crowley KA, Tan S, Denu JM, Peterson CL. Mol Cell 2002;10:935–942. [PubMed: 12419236]
36. Yu J, Li Y, Ishizuka T, Guenther MG, Lazar MA. EMBO J 2003;22:3403–3410. [PubMed: 12840002]
37. Zhang J, Kalkum M, Chait BT, Roeder RG. Mol Cell 2002;9:611–623. [PubMed: 11931768]
38. Gietz RD, Woods RA. Methods Enzymol 2002;350:87–96. [PubMed: 12073338]
39. Bradford MM. Anal Biochem 1976;72:248–254. [PubMed: 942051]
40. Laemmli UK. Nature 1970;227:680–685. [PubMed: 5432063]
41. Blacque OE, Worrall DM. J Biol Chem 2002;272:9950–9955.
42. Zargarian L, Le Tilly V, Jamin N, Chaffotte A, Gabrielsen OS, Toma F, Alpert B. Biochemistry 1999;38:1921–1929. [PubMed: 10026273]
43. Hwang SR, Steineckert B, Toneff T, Bundey R, Logvinova AV, Goldsmith P, Hook VY. Biochemistry 2002;41:10397–10405. [PubMed: 12173926]
44. Vincent MJ, Martin AS, Compans RW. J Biol Chem 1998;273:950–956. [PubMed: 9422755]
45. Townsley FM, Pelham HR. Eur J Cell Biol 1994;64:211–216. [PubMed: 7957309]
46. Teasdale RD, Jackson MR. Annu Rev Cell Dev Biol 1996;12:27–54. [PubMed: 8970721]
47. Rubin H, Wang ZM, Nickbarg EB, McLarney S, Naidoo N, Schoenberger OL, Johnson JL, Cooperman BS. J Biol Chem 1990;265:1199–1207. [PubMed: 2404007]
48. Gettins PG. Chem Rev 2002;102:4751–4804. [PubMed: 12475206]
49. Silverman GA, Bird PI, Carrell RW, Church FC, Coughlin PB, Gettins PG, Irving JA, Lomas DA, Luke CJ, Moyer RW, Pemberton PA, Remold-O'Donnell E, Salvesen GS, Travis J, Whisstock JC. J Biol Chem 2001;276:33293–33296. [PubMed: 11435447]
50. Luo Y, Zhou Y, Cooperman BS. J Biol Chem 1999;274:17733–17741. [PubMed: 10364215]
51. Duranton J, Adam C, Bieth JG. Biochemistry 1998;37:11239–11245. [PubMed: 9698370]
52. Kalsheker NA. Int J Biochem Cell Biol 1996;28:961–964. [PubMed: 8930118]
53. Hook VY, Tezapsidis N, Hwang SR, Sei C, Byrne M, Yasothornsrikul S. J Neurochem 1999;73:59–69. [PubMed: 10386955]
54. Zhou A, Carrell RW, Huntington JA. J Biol Chem 2001;276:27541–27547. [PubMed: 11325972]
55. Gooptu B, Hazes B, Chang WS, Dafforn TR, Carrell RW, Read RJ, Lomas DA. Proc Natl Acad Sci U S A 2000;97:67–72. [PubMed: 10618372]
56. Mahadeva R, Dafforn TR, Carrell RW, Lomas DA. J Biol Chem 2002;277:6771–6774. [PubMed: 11773044]
57. Jeppsson JO, Laurell CB, Fagerhol M. Eur J Biochem 1978;83:143–153. [PubMed: 304805]
58. Zupicich J, Brenner SE, Skarnes WC. Genome Biol 2001;2:research0050.1–research0050.6. [PubMed: 11790253]
59. Tahara E, Ito H, Taniyama K, Yokozaki H, Hata J. Hum Pathol 1984;15:957–964. [PubMed: 6207098]

60. Takada S, Tsuda M, Fujinami S, Yamamura M, Mitomi T, Katsunuma T. Cancer Res 1986;46:3688–3691. [PubMed: 3754789]

61. Naidoo N, Cooperman BS, Wang ZM, Liu XZ, Rubin H. J Biol Chem 1995;270:14548–14555. [PubMed: 7782318]

62. Travis J, Salvesen GS. Annu Rev Biochem 1983;52:655–709. [PubMed: 6193754]

63. Grigoryev SA, Bednar J, Woodcock CL. J Biol Chem 1999;274:5626–5636. [PubMed: 10026180]

64. Irving JA, Shushanov SS, Pike RN, Popova EY, Bromme D, Coetzer TH, Bottomley SP, Boulynko IA, Grigoryev SA, Whisstock JC. J Biol Chem 2002;277:13192–13201. [PubMed: 11821386]

65. Shoji W, Inoue T, Yamamoto T, Obinata M. J Biol Chem 1995;270:24818–24825. [PubMed: 7559602]

66. Inoue T, Shoji W, Obinata M. Genes Cells 2000;5:699–709. [PubMed: 10971652]

67. Braun EL, Grotewold E. Mol Biol Evol 2001;18:1401–1412. [PubMed: 11420378]

68. Yan W, Schilke B, Pfund C, Walter W, Kim S, Craig EA. EMBO J 1998;17:4809–4817. [PubMed: 9707440]

69. Zhang S, Lockshin C, Herbert A, Winter E, Rich A. EMBO J 1992;11:3787–3796. [PubMed: 1396572]

70. Hughes R, Chan FY, White RA, Zon LI. Genomics 1995;29:546–550. [PubMed: 8666407]

71. Kanei-Ishii C, Sarai A, Sawazaki T, Nakagoshi H, He DN, Ogata K, Nishimura Y, Ishii S. J Biol Chem 1990;265:19990–19995. [PubMed: 2246275]

72. Matsumoto-Taniura N, Pirollet F, Monroe R, Gerace L, Westendorf JM. Mol Biol Cell 1996;7:1455–1469. [PubMed: 8885239]

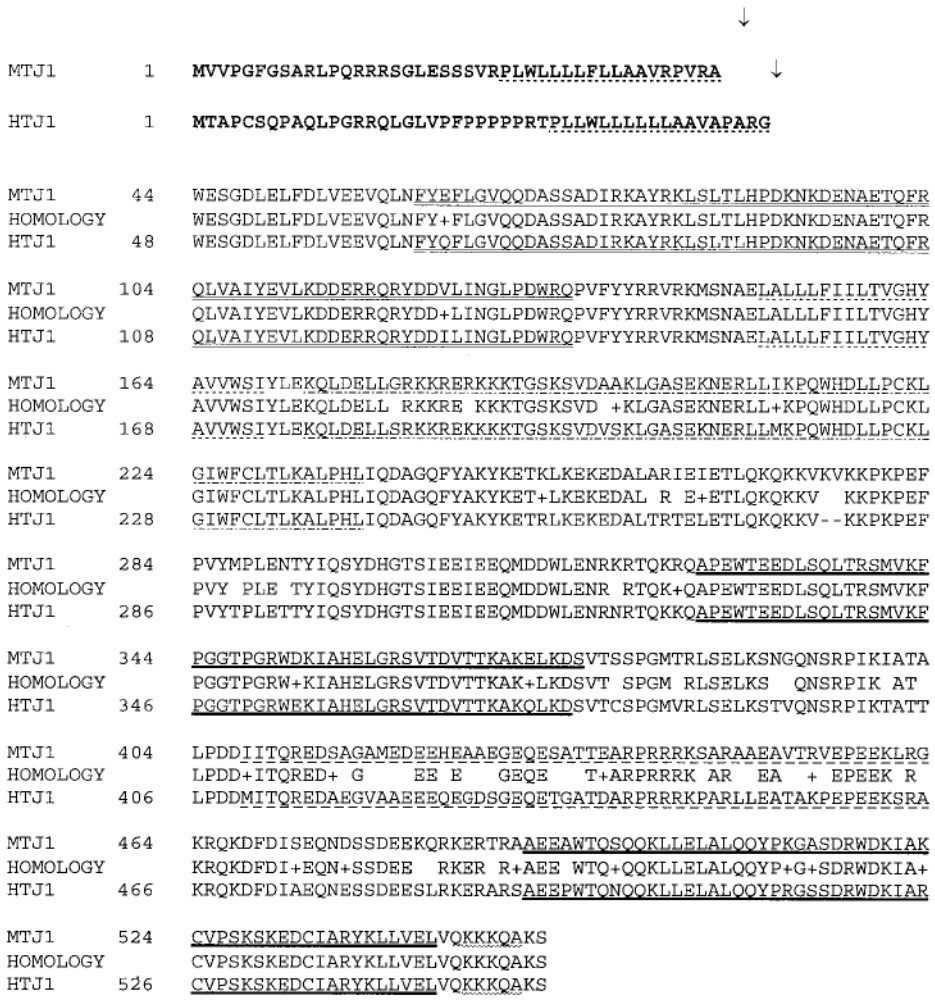

Fig. 1. Homology of the mouse MTJ1 (accession number L16953) with the human HTJ1 (accession number AY225122) and analysis of their amino acid sequences

Capital letters indicate amino acid identity, + indicates similarity. Gaps (−) have been introduced for maximum similarity. The signal peptide (*bold*) and cleavage site (*arrow*) were predicted with the program SignalP version 1. 1. The J-domain (*double underline*) and the SANT domains (*bold plain underline*) were predicted using the SMART program. The transmembrane domain (*dotted line*) was predicted by using the TMPRED program. The ribosome binding region identified recently (24) is *underlined* (*dot dashed*). The region that presents homology with the Sec63 (*dashed underline*) has been identified using the program SIM. The COOH-terminal endoplasmic reticulum retrieval signal (*wavy line*) was identified with the program PSORT II.

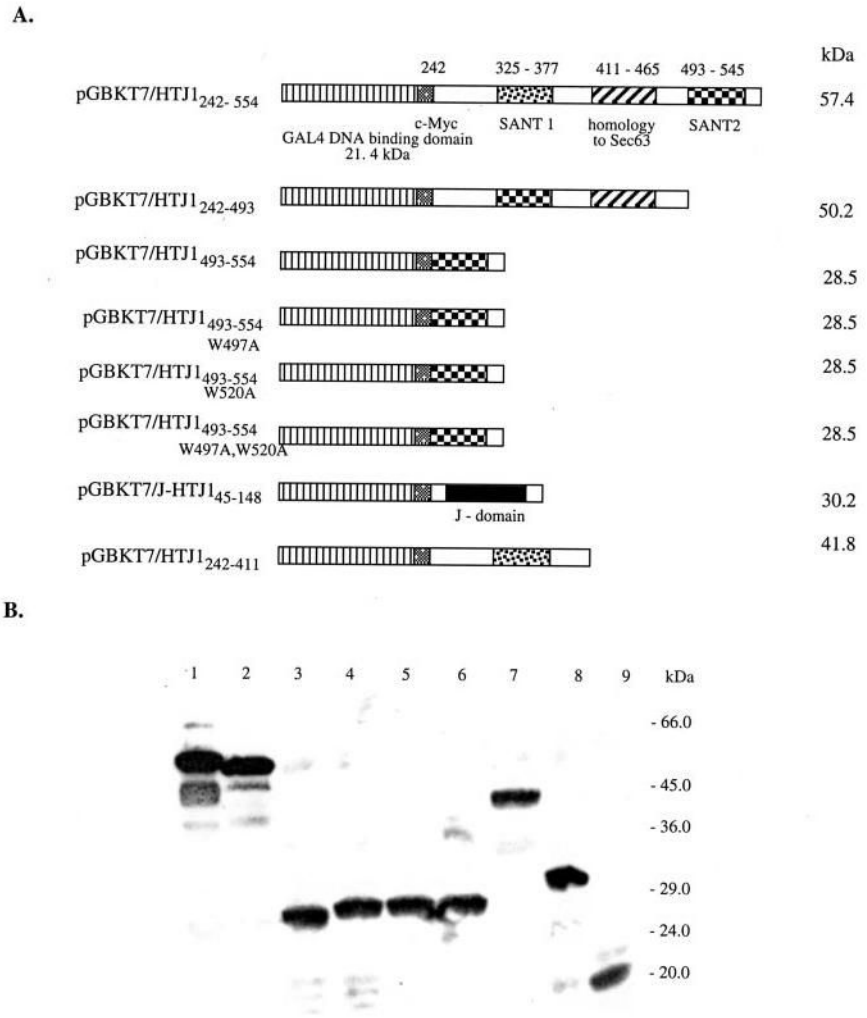

Fig. 2. Expression of HTJ1 fusion proteins with the GAL4 DNA-binding domain and the c-Myc epitope in yeast

A, schematic representation of HTJ1 constructs used in this study. The position of amino acids in HTJ1, the size in kDa, and the interaction with ACT are indicated. *B*, immunoblot of total yeast protein extracts. Protein extracts from the AH109 yeast strain transformed with (*lane 1*), pGBKT7/pGBKT7/HTJ1$_{242–554}$ HTJ1$_{242–493}$ (*lane 2*), pGBKT7/HTJ1$_{493–554}$ (*lane 3*), pGBKT7/HTJ1$_{493–554}$:W497A (*lane 4*), pGBKT7/HTJ1$_{493–554}$:W520A (*lane 5*), pGBKT7/HTJ1$_{493–554}$:W497A, W520A (*lane 6*), pGBKT7/HTJ1$_{242–411}$ (*lane 7*), pGBKT7/HTJ1$_{45–148}$ (*lane 8*), and pGBKT7 vector (*lane 9*) were separated on a 10% SDS-PAGE gel and detected with an anti-c-Myc monoclonal antibody.

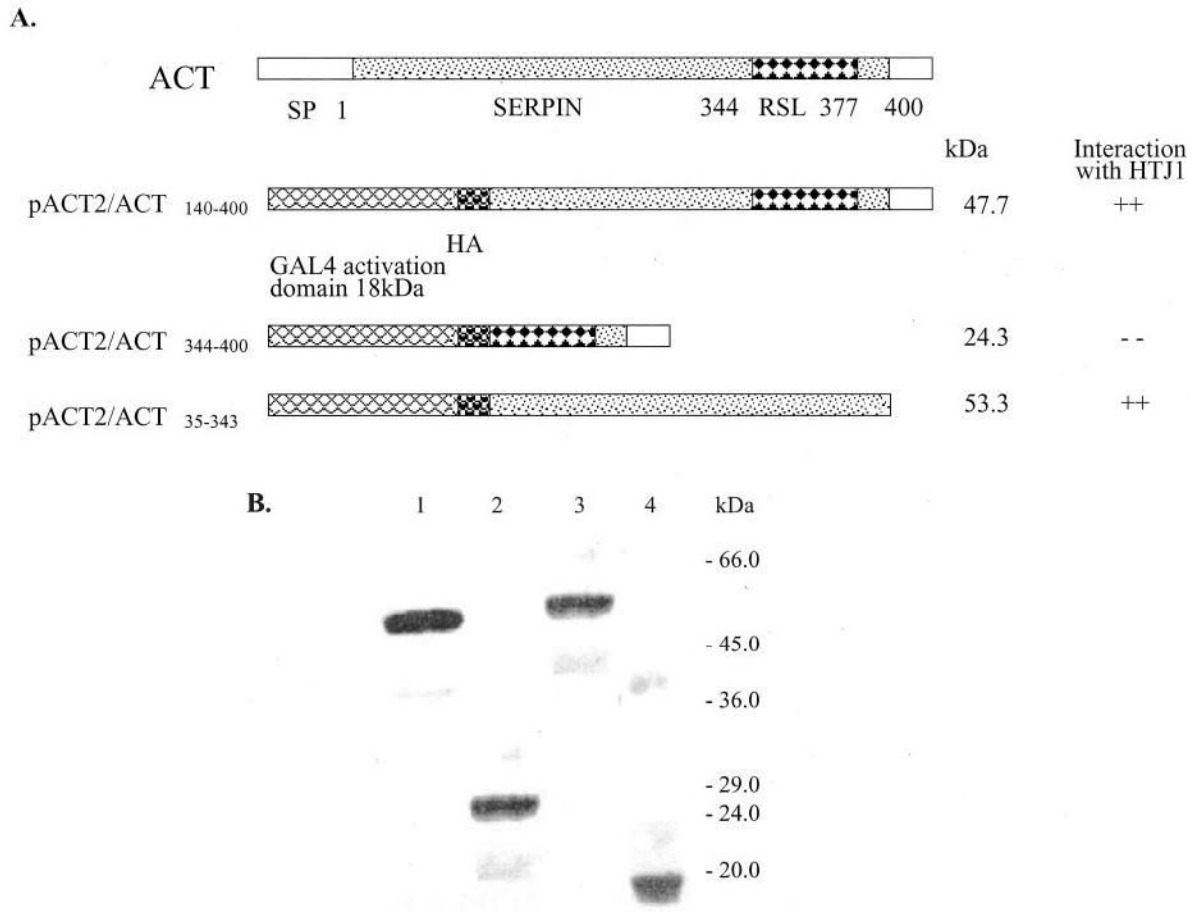

Fig. 3. Expression of ACT fusion proteins with the GAL4 activation domain and the HA epitope in yeast

A, schematic representation of human ACT constructs used in this study. The position of amino acids of ACT, the size in kDa, and the interaction with HTJ1 are indicated. Position 1 starts after the signal peptide (*SP*) cleavage site. *B*, immunoblot of total yeast protein extracts. Protein extracts from yeast transformed with pACT2/$ACT_{140–400}$ (*lane 1*), pACT2/$ACT_{344–400}$ (*lane 2*), pACT2/$ACT_{35–343}$ (*lane 3*), and pACT2 (*lane 4*) were separated on a 10% SDS-PAGE gel and detected with an anti-HA polyclonal antibody.

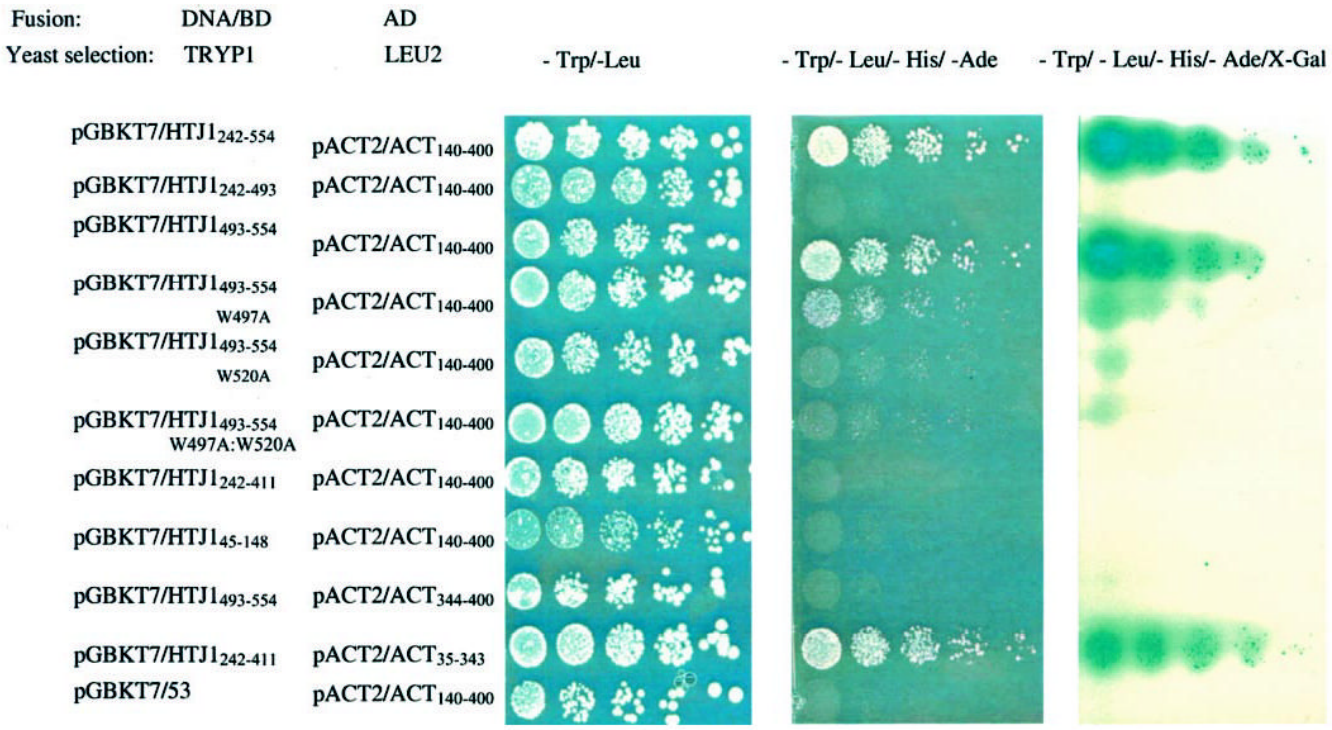

Fig. 4. Yeast two-hybrid one-on-one interactions

HTJ1 constructs fused to the Gal4 DNA-binding domain (described in Fig. 2) were individually analyzed for interaction with fragments of ACT expressed in yeast as a fusion with the Gal4 activation domain (see Fig. 3). The prey plasmids pACT2/$ACT_{140–400}$, pACT2/$ACT_{344–400}$, or pACT2/$ACT_{35–343}$ (*LEU2*) were co-transformed into the auxotrophic *S. cerevisiae* AH109 strain with bait plasmid containing HTJ1 truncated constructs (TRYP1). Double transformants were selected on selective medium depleted in tryptophan and leucine (−Trp/−Leu). Interaction between the bait (HTJ1) and the prey (ACT) brings the Gal4 activation domain (*AD*) and the DNA-binding domain (*DNA*/*BD*) into close proximity, resulting in the activation of the *HIS3*, *ADE2*, and *MEL1* reporter genes. Yeast cells harboring plasmids that code for interacting prey-bait pairs can grow on selective medium depleted in adenine and histidine (−Trp/−Leu/−Ade/−His) and turn blue in the presence of X-α-gal because of the expression of the MEL1 gene product (α-galactosidase).

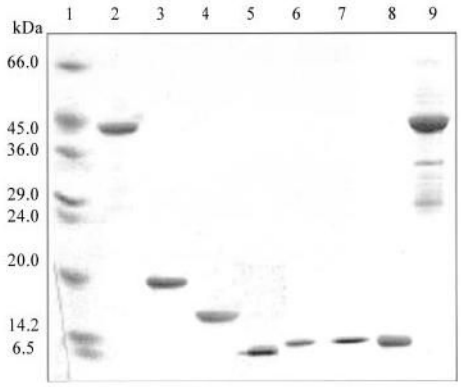

Fig. 5. SDS-PAGE analysis of purified HTJ1 and ACT variant proteins

Proteins were expressed in *E. coli* and purified by cobalt-chelating resin and gel filtration as described under "Experimental Procedures." Samples were analyzed on a 12.5% SDS-PAGE, and detected by staining with Coomassie Blue. *Lane 1*, standard molecular weight; *lane 2*, His_6-$HTJ1_{242–554}$ (~38 kDa); *lane 3*, His_6-$HTJ1_{242–377}$ (~18 kDa); *lane 4*, His_6-$HTJ1_{378–492}$ (~15 kDa); *lane 5*, His_6-$HTJ1_{493–554}$ (~9 kDa); *lane 6*, His_6-$HTJ1_{493–554}$:W497A (~9 kDa); *lane 7*, His_6-$HTJ1_{493–554}$:W520A (~9 kDa); *lane 8*, His_6-$HTJ1_{493–554}$: W497A,W520A (~9 kDa); *lane 9*, His_6-$ACT_{1–400}$ (~46 kDa).

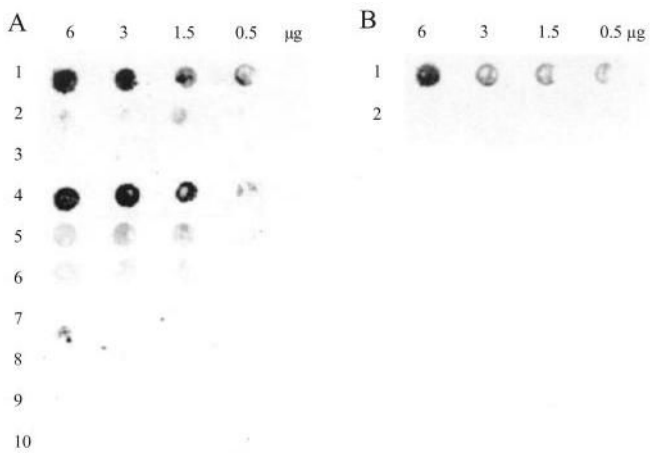

Fig. 6. Dot blot analysis of ACT binding to HTJ1 variants, BiP, and bovine serum albumin

A, nitrocellulose membrane was spotted with decreasing amounts of His_6-$HTJ1_{242–554}$ (*lane 1*), His_6-$HTJ1_{242–377}$ (*lane 2*), His_6-$HTJ1_{378–492}$ (*lane 3*), His_6-$HTJ1_{493–554}$ (*lane 4*), His_6-$HTJ1_{493–554}$:W497A (*lane 5*), His_6-$HTJ1_{493–554}$:W520A (*lane 6*), His_6-$HTJ1_{493–554}$:W497A,W520A (*lane 7*), His_6-JMTJ1 (*lane 8*), His_6-BiP (*lane 9*), and bovine serum albumin (*lane 10*). After blocking with 5% milk the membrane was incubated with His_6-ACT (5 µg/ml) overnight at 4 °C. Bound ACT was detected by immunostaining with an anti-ACT antibody as described under "Experimental Procedures." *B*, nitrocellulose membrane was spotted with decreasing amounts of His_6-J-MTJ1 (*lane 1*) and His_6-J-MTJ1:H89Q (*lane 2*) prior to incubation with His_6-BiP. Bound BiP was detected by immunostaining with anti-BiP antibody.

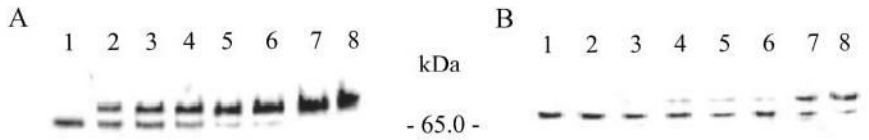

Fig. 7. ACT forms a stable complex with SANT2

Human plasma ACT (0.2 μM) was incubated with SANT2 (ACT-His_6-$HTJ1_{493–554}$, *panel* A) or SANT2:W497A (ACT-His_6-$HTJ1_{493–554}$:W497A, *panel B*) at a ACT:SANT2 molar ratio equal to 1:0 (*lane 1*), 1:1 (*lane 2*), 1:2 (*lane 3*), 1:5 (*lane 4*), 1:10 (*lane 5*), 1:20 (*lane 6*), 1:40 (*lane 7*), and 1:80 (*lane 8*). After electrophoresis in native conditions, proteins were transferred onto nitrocellulose membrane and ACT was detected by Western blotting.

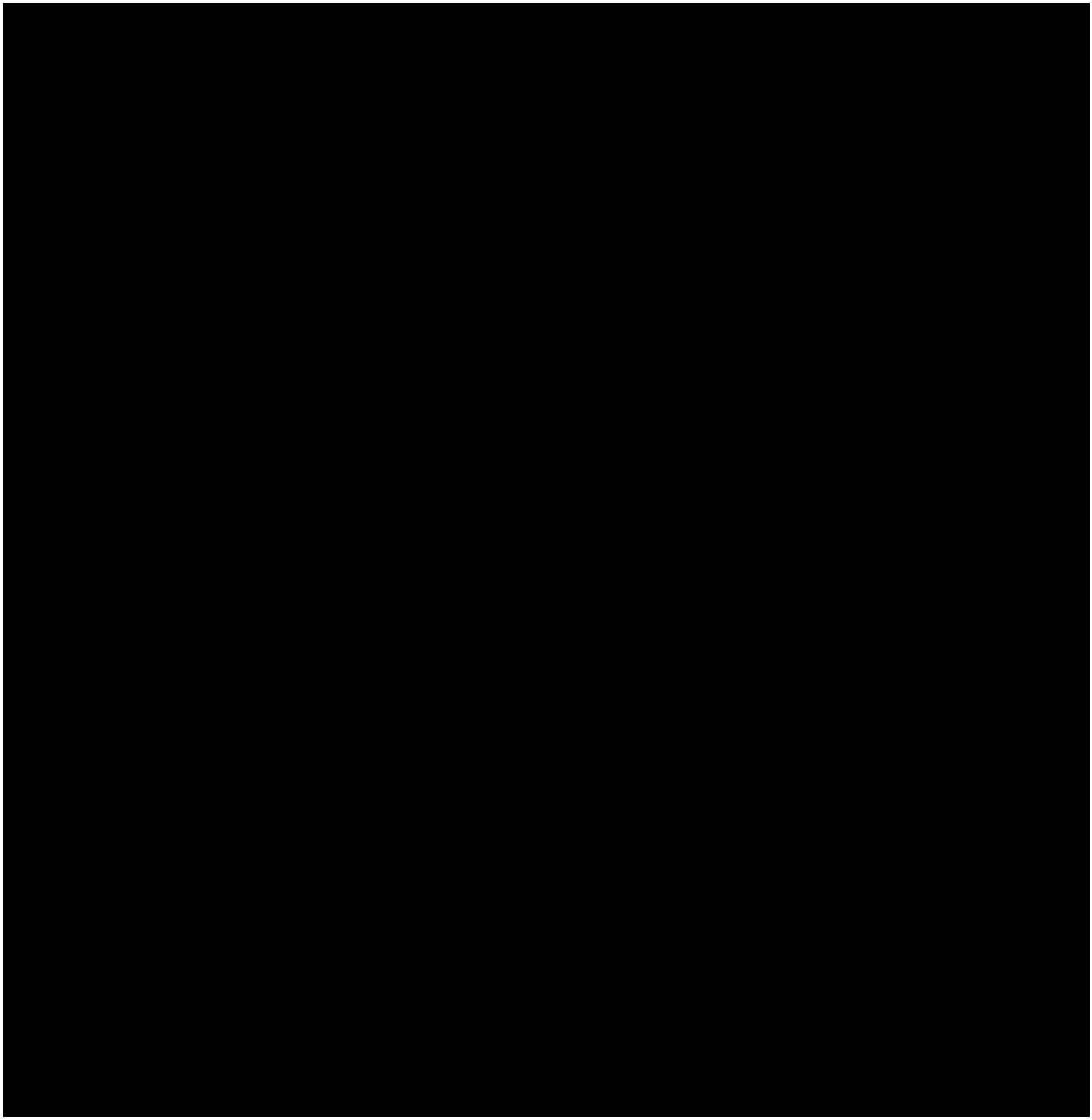

Fig. 8. Tryptophan fluorescence quenching of SANT2 upon ACT binding

A, corrected emission spectra of SANT2 (4 nM) alone (*open squares*) or in the presence of ACT at 0.5 nM (*dotted line*), 1 nM (*open triangles*), 4 nM (*closed squares*), or 16 nM (*closed triangles*). *B*, binding curve as a function of ACT concentration. *C*, Scatchard representation of the tryptophan fluorescence quenching of SANT2 upon ACT binding. *D*, Lehrer plot of the tryptophan fluorescence quenching of SANT2 (4 nM) by ACT.

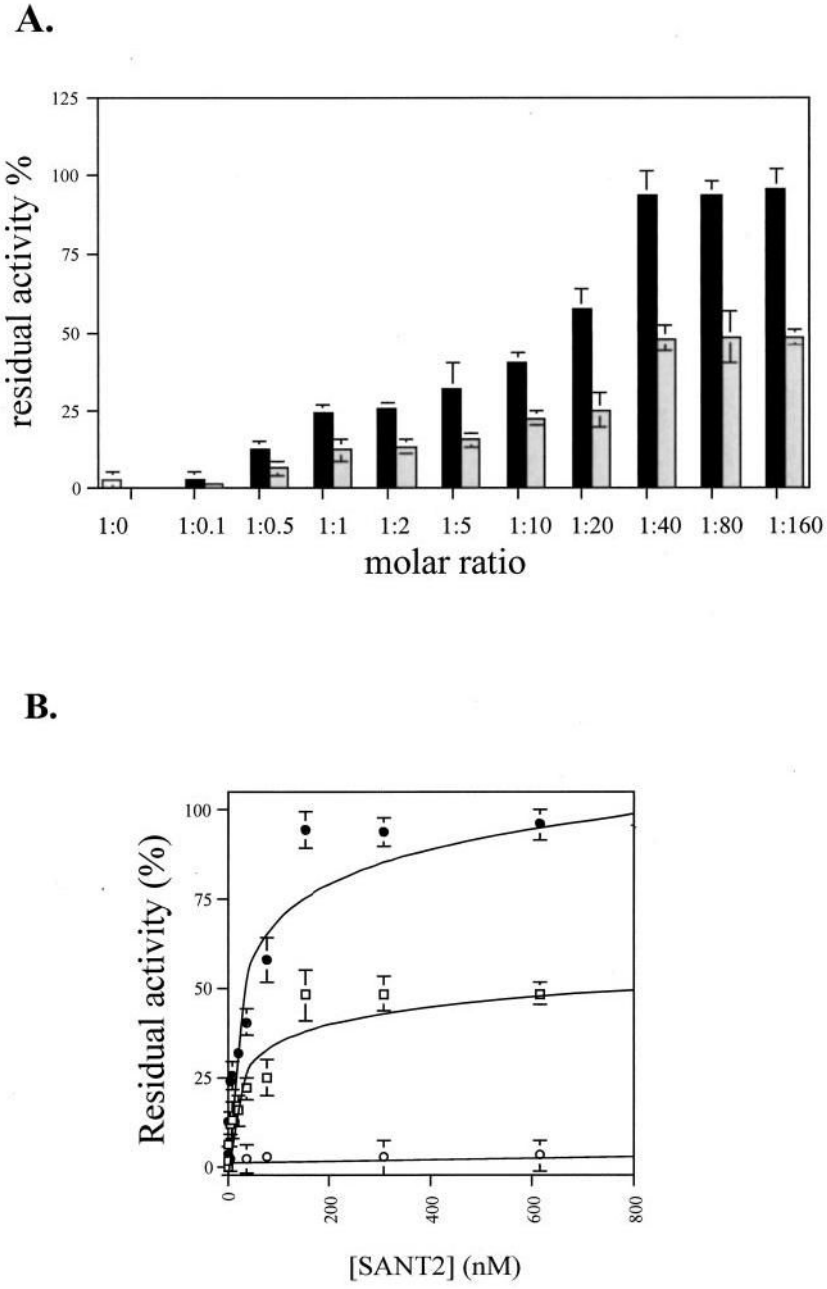

Fig. 9. Change in ACT inhibitory activity toward chymotrypsin following preincubation with SANT2

A, enzyme activity was measured as described under "Experimental Procedures" for 4.0 nM chymotrypsin in the presence of 4 nM ACT and His_6-$HTJ1_{493–554}$ (*dark graybars*) or the mutant His_6-$HTJ1_{493–554}$:W497A (*light gray bars*) at ACT:SANT2 molar ratios ranging from 1:0.1 to 1:160. The *bar* represents the mean of three independent determinations. *B*, human plasma ACT (4.0 nM) was incubated with increasing concentrations of His_6-$HTJ1_{493–554}$ (*closed circles*), the single mutant His_6-$HTJ1_{493–554}$:W497A (*open squares*), or the double mutant His_6-$HTJ1_{493–554}$:W497A,W520A (*open circles*) for 20 min at 25 °C, prior to the addition of chymotrypsin (4 nM) and the substrate Succ-AAPF-*p*NA at 0.1 mM. Absorbance at 405 nm was recorded as a function of time and the residual activity was normalized to chymotrypsin alone

(100%), which was unaffected by the presence of 320 n_M His_6-$HTJ1_{493–554}$ or His_6-$HTJ1_{493–554}$:W497A.

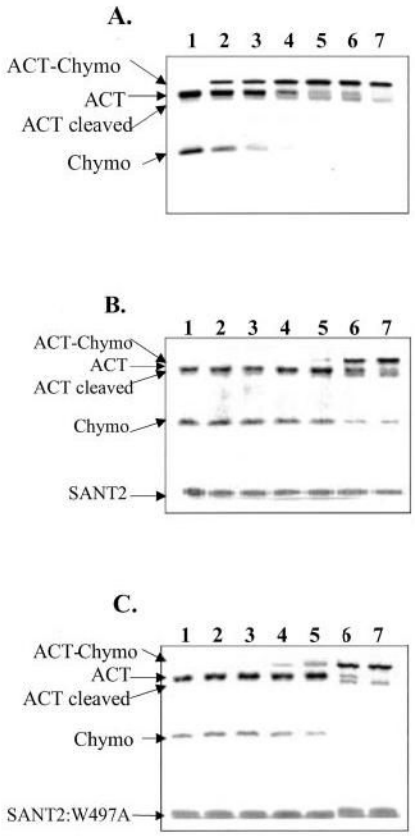

Fig. 10. Kinetics of formation of the ACT-chymotrypsin covalent complex in the absence or presence of SANT2

A, human plasma ACT (0.7 μM) was incubated with chymotrypsin (0.7 μM) at 25 °C in 20 mM Tris (pH 8.0), 100 mM NaCl, and 0.1 mM Succ-AAPF-*p*NA for 0, 5, 10, 20 s, and 1, 5, and 10 min (*lanes 1–7*, respectively). At each time interval, an aliquot was taken and the reaction was stopped by addition of 0.5 mM phenylmethylsulfonyl fluoride, 2-fold dilution in 0.125M Tris-HCl, 4% SDS, 20% (v/v) glycerol, 0.02% bromphenol blue (pH 6.8), and transfer to 4 °C. Samples were analyzed by 15% SDS-PAGE and Coomassie staining. The same experiment was performed in the presence of 14 μM SANT2 (*B*) or 14 μM SANT2:W497A (*C*).

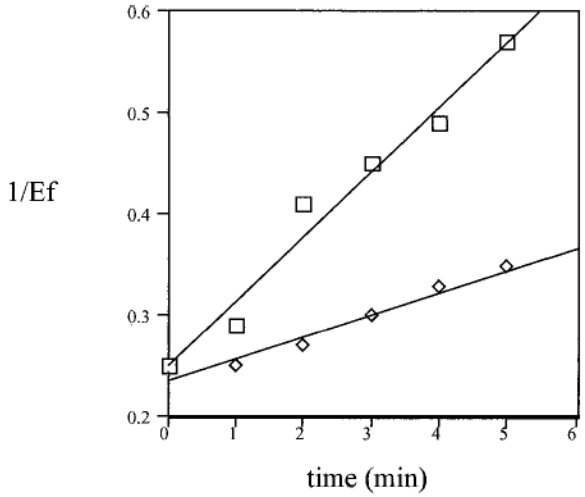

Fig. 11. Kinetic analysis of ACT inhibition of chymotrypsin

The residual activity of chymotrypsin (4 n_M) in the presence of ACT alone (*open squares*) or in the presence of 4 n_M SANT2 (*open diamonds*) was measured at timed intervals as described under "Experimental Procedures."

Table I

Primer sequences and templates for PCR, and restriction sites for cloning

Restriction sites are underlined; positions mutated are in boldface.

Forward primer	Reverse primer	Restriction sites	Construct name	Template
5′-CATGCCATGGATCCAGGATGCT GGGCAGTTTTATGC-3′	5′-TCAGCTTTTAGCTTGTTTTTTCTTTTGGACC-3′	NcoI-SmaI	pGBKT7/ $HTJ1_{242-554}$	pUCHTJ1
5′-CATGCCATGGATCCAGGATGCTGGGCAGTTTTATGC-3′	5′-CGGGATCCGATCATGTCATCGGGCAAGGTG-3′	NcoI-BamHI	pGBKT7/ $HTJI_{242-411}$	pUCHTJI
5′-GGAATTCCATATGGCAGAGGAGCCGTGGACTCAAAATC-3′	5′-CCGCTCGAGTCAGCTTTTAGCTTGTTTTTTCTTTTGGACCAG-3′	NdeI-SmaI	pGBKT7/ $HTJI_{493-554}$	pUCHTJI
5′-GGAATTCCATATGGCAGAGGAGCC**GGC**GACTCAAAATC-3′	5′-CCGCTCGAGTCAGCTTTTAGCTTGTTTTTTCTTTTGGACCAG-3′	NdeI-SmaI	pGBKT7/ $HTJI_{493-554}$:W497A	pGBKT7/ $HTJI_{493-554}$
5′-CTCTGACCGC**GCG**GACAAAA-	5′-CTATTTTGTC**CGC**GCGGTCAGAG-3′	NA[a]	pGBKT7/ $HTJI_{493-554}$:W520A	pGBKT7/ $HTJI_{493-554}$
5′-CTCTGACCGC**GCG**GACAAAATAG-3′	5′-CTATTTTGTC**CGC**GCGGTCAGAG-3′	NA	pGBKT7/ $HTJI_{493-554}$W497A: W520A	pGBKT7/ $HTJI_{493-554}$: W497A
5′-GGAATTCCATATGGCGCGCGCGGCTGGGAGAGCGGAGAC-3′	5′-TTTTCTCACCCGCCTGTAGTAGAATAC-3′	NdeI-SmaI	pGBKT7/J- $HTJI_{45-148}$	pUCHTJ1
5′-GGAATTCCATATGATCCAGGATGCTGGGCAGTTTTATGC-3′	5′-CCGCTCGAGTCAGCTTTTAGCTTGTTTTTTCTTTTGGACCAG-3′	NdeI-XhoI	p(His)$_6$-$HTJI_{242-554}$	pUCHTJI
5′-GGAATTCCATATGGTGACAGATGTGACAACCAAAGC-3′	5′-CCGCTCGAGAGACCGAGCTCTCTCTTTTCTC-3′	NdeI-XhoI	p(His)$_6$-$HTJI_{378-492}$	pUCHTJI
5′-GGAATTCCATATGATCCAGGATGCTGGGCAGTTTTATGC-3′	5′-CCGCTCGAGAGATCGACCCAATTCGTGGGCAATC-3′	NdeI-XhoI	p(His)$_6$-$HTJI_{242-177}$	pUCHTJI
5′-GGAATTCCATATGCACCCTTAACAGCCCACTTGACGAG-3′	5′-CGGGATCCCTAGGCTTGCTTGGGATTGGTG-3′	NdeI-BamH1	p(His)$_6$-ACT_{1-400}	cDNA human liver library
5′-CGGGATCCGAGAGGAGGGCACAGAAGCATC-3′	5′-CGGAATTCTTACTAGGCTTGCTTGGATTGGTG-3′	BamH1-EcoR1	pACT2/$ACT_{144-400}$	p(His)$_6$-ACT_{1-100}
5′-CCCCCCGGGGTTCAGCCTGTACAAGCAGTTAGTC-3′	5′-CGGAATTCAATTAAAATACATCAAGCACAGCC-3′	Xma1-EcoR1	pACT2/ACT_{35-343}	p(His)$_6$-ACT_{1-400}

[a] NA, not applicable.

Table II

Kinetic and catalytic properties of chymotrypsin in the presence of SANT2

All constants were determined as described under "Experimental Procedures."

	k_{cat}	K_m	k_{cat}/K_m	k_{ass}
	s^{-1}	μM	$M^{-1}\ s^{-1}$	
Chymotrypsin	20.3	58	0.35×10^6	6.5×10^5
Chymotrypsin with SANT2	20.9	57	0.36×10^6	3.5×10^5